Stable isotope evidence for crustal recycling as recorded by superdeep diamonds

A.D. Burnham[1,2]*, A.R. Thomson[1,3], G.P. Bulanova[1], S.C. Kohn[1], C.B. Smith[1], M.J. Walter[1]

1 – School of Earth Sciences, University of Bristol, Wills Memorial Building, Bristol, BS8 1RJ, UK.
2 – (present address) Research School of Earth Sciences, Australian National University, Canberra ACT 2601, Australia
3 – (present address) Department of Earth Sciences, University College London, WC1E 6BT, UK.
* corresponding author, email antony.burnham@anu.edu.au

Abstract

Sub-lithospheric diamonds from the Juina-5 and Collier-4 kimberlites and the Machado River alluvial deposit in Brazil have carbon isotopic compositions that co-vary with the oxygen isotopic compositions of their inclusions, which implies that they formed by a mixing process. The proposed model for this mixing process, based on interaction of slab-derived carbonate melt with reduced (carbide- or metal-bearing) ambient mantle, explains these isotopic observations. It is also consistent with the observed trace element chemistries of diamond inclusions from these localities and with the experimental phase relations of carbonated subducted crust. The ^{18}O-enriched nature of the inclusions demonstrates that they incorporate material from crustal protoliths that previously interacted with seawater, thus confirming the subduction-related origin of superdeep diamonds. These samples also provide direct evidence of an isotopically anomalous reservoir in the deep (≥ 350 km) mantle.

1. Introduction

Diamonds, the deepest-derived mineral grains available for scientific study, have long been used to provide insights into the nature of the mantle and chemical processes in the deep Earth. A key indicator of diamond provenance is the mineralogy and composition of trapped inclusions, the majority of which indicate diamond formation in the lithospheric mantle; a small proportion (<5 %) of diamonds formed at much higher pressures, deep in the asthenospheric upper mantle or even the lower mantle (Stachel et al., 2005; Walter et al., 2011; Kaminsky, 2012).

Subduction of oceanic lithosphere returns material (sea-floor sediments, altered lavas and depleted mantle rocks) from the Earth's surface to the mantle. The fate of the various subducted lithologies remains enigmatic, with questions still unanswered regarding the extent to which these materials might be decoupled, how deep material descends into the mantle, and the extent to which subducted material is isolated from the convecting mantle. For example, subducted crust may be incorporated into the sub-cratonic lithosphere as demonstrated by mantle xenoliths and diamonds transported to the surface by kimberlite eruptions worldwide (Jacob, 2004), or it may mix back into the mantle as suggested by seismic tomography showing slabs stalled at the 660 km discontinuity and even penetrating into the lower mantle (Widiyantoro et al., 1999).

Oxygen isotopes are a powerful tracer of crustal material, only being fractionated significantly at low temperatures (Bindeman, 2008). Hence, any value outside a narrow "peridotitic mantle" range, $\delta^{18}O_{SMOW} = 5.7 \pm 0.2$ ‰, is diagnostic of a shallow crustal origin. For example, $\delta^{18}O$ values lie in the range 11-21 ‰ for mudrocks (Land and Lynch, 1996), 20-35 ‰ for marine limestones (Land and Lynch, 1996) and 3-15 ‰ for altered basaltic lavas (Gregory and Taylor, 1981). Studies of the oxygen isotopic compositions of silicates (Lowry et al., 1999; Schulze et al., 2004; Ickert et al., 2013; Schulze et al., 2013) and the sulphur isotopic ratios of sulphides (Farquhar et al., 2002) within lithospheric diamonds testify to the subducted origin of some mineral inclusions in lithospheric diamonds. The isotopic composition of C in diamond similarly has a narrow isotopic range within typical peridotitic mantle, with $\delta^{13}C_{PDB}$ around -5 ± 1 ‰ (Ickert et al., 2013). Lithospheric diamonds hosting eclogitic silicate inclusions often show a co-variation between the $\delta^{13}C$ of the former and the $\delta^{18}O$ of the latter, as shown in Figure 1 (Lowry et al., 1999; Ickert et al., 2013; Schulze et al., 2013). Such examples indicate that not all subducted material is recycled back into the convecting mantle, but can instead be incorporated into or accreted onto the lithospheric mantle. Those rare "superdeep" diamonds that originate in the convecting mantle beneath the lithosphere provide a direct insight into the mineralogy and geochemistry of the deep mantle. Ickert et al. (2015) reported the O isotopic compositions of majorite inclusions in diamonds from South Africa (the Jagersfontein kimberlite). As with lithospheric

eclogitic inclusions from other localities worldwide, these are enriched in $\delta^{18}O$ (Fig. 1), indicative of the crustal nature of the protolith.

Here we report the relationship between $\delta^{13}C$ and $\delta^{18}O$ for superdeep diamonds from Brazil (the Juina-5 and Collier-4 kimberlites; Bulanova et al., 2010; Walter et al., 2011; Thomson et al., 2014 and the Machado River alluvial deposit; Bulanova et al., 2008). We use these data to test the hypothesis that many superdeep diamonds are formed from recycled material. Additionally we assess the extent to which isotopic signatures of crustal materials are maintained throughout their passage into the deep mantle, rather than being removed and re-homogenised during the subduction process that includes dehydration and sediment melting. Although the suites of diamonds studied contain a wide variety of deep upper mantle minerals, the calibration of $\delta^{18}O$ by ion probe secondary ion mass spectroscopy (SIMS) varies considerably and unpredictably between minerals. Because of this limitation, only coesite, $CaSiO_3$-walstromite and garnet were analysed.

2. Methods

Inclusion-bearing diamonds were polished to expose the inclusions at the surface, mounted in indium and gold-coated. Mineral structures were verified by Raman spectroscopy using a Thermo Scientific DXRxi microscope equipped with a 455 or 532 nm excitation laser. Panchromatic cathodoluminescence (CL) images were recorded using a Hitachi S-3500N scanning electron microscope. Backscattered electron imaging and electron probe microanalysis of the major element composition were performed using a JEOL JXA8530F Hyperprobe operating at 20 kV and 3 nA (imaging) or 20 nA (compositional analysis by wavelength dispersive spectroscopy).

SIMS analysis of carbon and oxygen isotopic ratios was carried out at the Edinburgh Ion Microprobe Facility (EIMF) using a Cameca 1270 mass spectrometer operating at 10 kV and 6 nA primary Cs^+ beam current. Electron flooding minimised charge build-up during the measurement of O isotope ratios. In-house standards were used for calibration and drift correction. The standard for diamond was synthetic diamond SYN ($\delta^{13}C$ = -23.9 ‰), that used for coesite was Bogala quartz ($\delta^{18}O$ = 12.3 ‰; there

is no instrumental mass fractionation (IMF) difference between quartz and coesite, Schulze et al., 2003) and for $CaSiO_3$ a synthetic Ca-walstromite was prepared at 3.1 GPa and 1580 °C in a piston cylinder apparatus, and characterised for $\delta^{18}O$ by laser fluorination at SUERC as $\delta^{18}O$ = 21.0 ± 0.4 ‰ (1σ, *n* = 4). For garnet a set of 10 standards of known $\delta^{18}O$ were analysed to provide a working curve for the instrumental mass fractionation as a function of composition, with garnet 13-63-44 (Page et al., 2010) analysed throughout the session to monitor instrument drift. $\delta^{18}O$ was parameterised as a quadratic function of the Ca content of the garnet (Page et al., 2010). For the first analytical session this gave $\delta^{18}O_{sample} = \delta^{18}O_{drift\ corrected} + 0.652*(X_{Ca})^2 - 2.98*(X_{Ca}) + 1.34$, which had a mean deviation from the observed IMF of 0.23 ‰. The larger garnet in ColN-18 was analysed the following day, on which occasion the IMF was ~ 0.29 ‰ smaller. However, the relative IMFs of the garnets studied were in excellent agreement with previous measurements made at EIMF using similar instrumental setup and differed only in the constant in the IMF equation, and hence this analysis was corrected using $\delta^{18}O_{sample} = \delta^{18}O_{drift\ corrected} + 0.652*(X_{Ca})^2 - 2.98*(X_{Ca}) + 1.05$. The standards available contained negligible Na and Ti which, respectively, are present at up to 0.19 and 0.09 atoms per formula unit (12 oxygens) in the diamond inclusions. Treating the Na component as identical to Ca for the diamond inclusions would result in $\delta^{18}O_{sample}$ values that were lower by at most 0.39 ‰ (mean = 0.19 ‰) and therefore the neglect of this component is probably not significant. The Ti component of the garnet is lower than that of Na, and was ignored. Overall, we estimate the uncertainty of our garnet measurements as the combination of the spot-to-spot reproducibility, 0.15 ‰ (an average of 0.18 ‰ for the drift-affected morning session (*n* = 25) and 0.13 ‰ for the more stable afternoon session (*n* = 20)), and the mean deviation of the IMF-corrected measurements from the accepted values for those materials, 0.23 ‰. Therefore we consider the 1σ uncertainty for the garnet $\delta^{18}O$ measurements to be 0.28 ‰. For coesite the spot-to-spot 1σ uncertainty was 0.14 ‰. For $CaSiO_3$ the uncertainty is dominated by the apparent inhomogeneity of the standard. This was tested in two sessions. During the first the spot-to spot reproducibility was 0.63 ‰ (*n* = 40) and during the second it was 0.57 ‰ (*n* = 20); excluding two markedly different values from the first session and one from the second improves the spot-to spot reproducibility to 0.44 ‰ and 0.31 ‰ respectively. These extreme outliers are probably related to the presence of decompression cracks within the synthetic material. The uncertainty on the laser fluorination value for the synthetic Ca-walstromite is

~ 0.37 ‰; combining this with the average reproducibility on the standard (0.38 ‰) gives an overall uncertainty of 0.53 ‰.

CL images were obtained after SIMS analysis to determine the internal structures of the samples and to verify the location of analytical points within the growth zones of the diamonds.

3. Results

The diamonds and inclusions studied are summarised in Table 1. EPMA data for the garnets are given in Table 2. The coesite inclusions are almost pure SiO_2 with trace amounts (< 0.06 wt%) of Al_2O_3 and TiO_2; the Ca-walstromite is almost pure endmember $CaSiO_3$ with other components comprising < 0.8% by weight (Table 3). Coesite with exsolved kyanite (Fig. 2a) probably formed as stishovite, which can accommodate much higher Al concentrations than other SiO_2 polymorphs (Liu et al., 2007), and must have formed at pressures above ~ 9 GPa (Zhang et al., 1993), equivalent to a minimum crystallisation depth of 270 km. The garnets have eclogitic compositions with a majoritic component and often have a rim of exsolved clinopyroxene (Fig. 2b). Several Ca-walstromite grains contain a small proportion (< 10 %) of exsolved $CaTiO_3$ grains (Fig. 2c), implying formation as $Ca(Si,Ti)O_3$ perovskite at pressures above ~ 12 GPa (Kubo et al., 1997). Minimum formation depths for the inclusions are taken to be 270 km for coesite, 230 km for garnet and 360 km for Ca-walstromite. The concentration of N in the diamonds, where measured, is typically low, and cathodoluminescence images (Fig. 3) show complex, diffuse internal zonation textures that are suggestive of a superdeep origin (Bulanova et al. 2010). All lines of evidence point to a related, sub-lithospheric, origin for the diamonds studied. The diamonds have $\delta^{13}C$ values from -26.4 ± 0.1 to -2.8 ± 0.1 ‰ and all measurements are consistent with previously published data for these and other samples from the same localities (Bulanova et al. 2008, 2010, Thomson et al., 2014). Mineral inclusion $\delta^{18}O$ values range from 7.5 ± 0.3 to 12.9 ± 0.3 ‰ and are anti-correlated with $\delta^{13}C$ of the host diamonds (Fig. 4); the ranges for all minerals overlap.

4. Discussion

Equilibrium oxygen isotope fractionation between coesite (and presumably stishovite) and garnet at temperatures above 1200 °C is below 1 ‰ (Sharp et al., 1992) and hence all inclusions are considered to be equally representative of the original lithology; likewise, exsolution is not expected to affect the $\delta^{18}O$ of the analysed phases. $\delta^{18}O$ values for all samples are significantly above the normal mantle range but within the range for crustal materials, and are at the higher end of the range of those previously obtained from eclogitic inclusions in lithospheric diamonds. Such high values suggest that the inclusions represent exceptionally well-preserved former crustal material that has survived isotopic modification to > 350 km depth.

Trace element data and phase relations suggest the Juina-region superdeep diamonds formed from melt released during partial melting of a carbonated slab at depths of 300-800 km (Walter et al., 2008; Bulanova et al, 2010). At these depths the mantle is highly reduced, with native Fe and/or Fe-carbide (e.g. Fe_3C or Fe_7C_3) present; the oxidised, carbonate-rich melts escaping from a subducted slab are expected to react with these reduced minerals in a "redox freezing" mechanism (Rohrbach and Schmidt, 2011):

$$3\,MgCO_3 + 2\,Fe_3C = 9\,Fe^{2+}_{0.67}Mg_{0.33}O + 5\,C$$

in melt *carbide* *in silicates* *diamond*

and

$$MgCO_3 + 2\,Fe = 3\,Fe^{2+}_{0.67}Mg_{0.33}O + C$$

in melt *metal* *in silicates* *diamond*

These reactions have several consequences. (i) Removal of carbonate from the melt dramatically raises its solidus, causing the other components of the melt (predominantly SiO_2+MgO+CaO+Na_2O) to crystallise out rapidly. (ii) FeO produced by the reaction will be incorporated into ferromagnesian mineral solid solutions such as garnet, bridgmanite and ferropericlase/magnesiowüstite. (iii) Isotopically light carbon ($\delta^{13}C$ < -5 ‰) in the melt will mix with mantle carbon ($\delta^{13}C$ = -5 ‰) in the carbide (or dissolved in solid solution within an Fe-Ni alloy) creating diamonds with intermediate isotopic compositions. (iv) Isotopically heavy oxygen ($\delta^{18}O$ > 6 ‰) in the melt will mix with mantle oxygen

($\delta^{18}O$ = 5.7 ‰) when the FeO and crystallised former melt components produced by the redox freezing reaction enter solid solution with and/or react with the surrounding mantle silicate phases.

The simultaneous operation of processes (iii) and (iv) will give rise to a mixing line between mantle and slab components. The general form of a two-component mixing line is a hyperbola most simply described by a pair of parametric equations:

$$\delta^{13}C_{mix} = \frac{\delta^{13}C^{melt} \cdot X_C^{melt} \cdot x + \delta^{13}C^{mantle} \cdot X_C^{mantle} \cdot (1-x)}{X_C^{melt} \cdot x + X_C^{mantle} \cdot (1-x)}$$

and

$$\delta^{18}O_{mix} = \frac{\delta^{18}O^{melt} \cdot X_O^{melt} \cdot x + \delta^{18}O^{mantle} \cdot X_O^{mantle} \cdot (1-x)}{X_O^{melt} \cdot x + X_O^{mantle} \cdot (1-x)}$$

where x and $(1 - x)$ are the proportions of slab melt and mantle component, respectively, and X_i is the concentration of element i in either the slab melt or the ambient mantle. With only two variables ($\delta^{13}C$ of the diamond and $\delta^{18}O$ of inclusions) measured directly, assumptions must be made about the isotopic and chemical compositions of the end-members to model the mixing hyperbola. The chemical composition of the carbonate melt is reasonably well constrained by experimental studies, with values of X_C^{melt} = 15.1 atomic % and X_O^{melt} = 60.1 atomic % (average values from the 1300 °C, 13 GPa and 1400 °C, 17 GPa experiments of Kiseeva et al., 2013). The mantle is accepted to have an isotopic composition of $\delta^{13}C^{mantle}$ = -5 ‰ and $\delta^{18}O^{mantle}$ = 5.7 ‰ (Bindeman, 2008, Ickert et al., 2013); values of $\delta^{13}C^{melt}$ = -26 ± 1 ‰ and $\delta^{18}O^{melt}$ = 11.25 ± 0.25 ‰ for the slab melt endmember are obtained by visual inspection of the data. The remaining two parameters, X_C^{mantle} and X_O^{mantle}, relate to the portion of the mantle reacting with the carbonate melt. We envisage this "effective reaction mixture" as containing both the Fe-carbide or metal involved in the redox reaction and neighbouring silicate grains (e.g. $(Mg,Fe)_2SiO_4$ polymorphs) that are close enough to exchange O isotopes diffusively or by dissolution/precipitation reactions. The best fit to the data suggests that the molar ratio Fe_3C/silicate (modelled as Mg_2SiO_4 for simplicity) must, on average, lie in the range 2 to 3.5 (Figure 4); if Fe metal containing minor dissolved C is the reductant the ratio must be considerably higher. The wide range of C-rich phases within oceanic crust and their highly variable isotopic compositions (Shilobreeva et al.,

2011) mean that other fits to the data are possible. The scatter of the data is attributed to a combination of variations in $\delta^{13}C^{melt}$ and $\delta^{18}O^{melt}$ arising from heterogeneity in the slab and "effective reaction mixtures" that will depend on the nature of the reactive flow of carbonate melts through the mantle, and on local thermal, chemical and textural conditions. In other words, it is to be expected that a suite of mixing lines will be in operation, resulting in a "mixing field"; four such mixing lines are shown in Figure 4. However, although our simple model is not the only possible explanation of the data the key observations are (i) that the inclusions are isotopically heavy in oxygen and hence must be derived largely from crustal material; (ii) the correlation cannot be explained by fractionation, which would result in a positively sloped correlation (Ickert et al., 2013).

The mass balance of the redox reaction between carbonate melt and metal or carbide proposed here can be calculated in two ways. Firstly, if the process is considered in terms of a direct local replacement of Fe or Fe_3C grains by diamond, how large would the grains have to be? Assuming a spherical geometry with a typical diamond diameters in the range 2.5 – 3 mm and taking into account the stoichiometry of the reaction and the relative densities, but ignoring the effects of resorption, the grain size of Fe metal or Fe_3C would be ~ 4.5 and 4 mm respectively. The actual grain size of Fe or Fe_3C in the mantle is unknown, but these figures seem reasonable given the grain size of silicate minerals in mantle xenoliths. The second way to consider the issue of mass balance is to start from the expected proportion of metal in peridotite at appropriate mantle depths, which is 50 – 700 ppm by weight (Rohrbach et al., 2014), and calculate the maximum possible diamond grade of the mantle source rock. This range of Fe abundances would give a diamond grade between 27 and 376 ct/tonne which is an abundant excess compared to the observed value of 0.40 ct/tonne in the Collier-4 kimberlite (Kaminsky et al., 2010). Therefore, even if resorption is taken into account there is likely to be sufficient reductant present in the mantle to account for the formation of these diamonds.

It was suggested by Luth and Stachel (2014) that diamond formation in the lithosphere is unlikely to be controlled by reduction of Fe^{3+} to Fe^{2+} because there is too little buffering potential in such reactions; diamond precipitation as a result of cooling and depressurising C-H-O fluids was proposed instead.

Such a mechanism would not explain the observations of the present study: the curvature of the mixing line requires the "effective reaction mixture" to have a higher C/O ratio than the slab-derived melt, a feature that is best explained by carbide and/or C-bearing metal predominating at the site of diamond crystallisation. The concerns raised by Luth and Stachel (2014) should, however, be taken into consideration when attempting to explain the relationships between $\delta^{13}C$ and $\delta^{18}O$ for lithospheric diamonds (e.g. Ickert et al., 2013), which are similar to that in the present study but must have a different origin.

Our model is consistent with the $\delta^{13}C$ zonation observed in Juina-5 and Collier-4 diamonds. Although the zonation varies (Bulanova et al. 2010; Thomson et al. 2014), nearly all the diamonds that contain very light carbon (-22 to -27 ‰) are either unzoned or have a light core and heavier rim. This suggests initial diamond growth from a fluid dominated by the crustal-derived carbon component, and progressive dilution of crustal carbon in the fluid with mantle carbon as the mixing process and diamond growth progress together. Although $\delta^{13}C_{PDB} \sim 0$ is typical for carbonates, whether they are hydrothermal (e.g. Alt and Teagle, 2003) or sedimentary (Hudson, 1977), and the low values proposed in the present study are more characteristic of organic material, isotopically-light C is known from CO_2 in fluid inclusions in a number of high-pressure metamorphic rocks (Nadeau et al., 1993; Yang et al., 2001). These lighter values presumably arise by metamorphism of precursor organic carbon. Serpentinite breakdown has been linked to the generation of oxidised fluids (Debret et al., 2015); we suggest that this and other metamorphic processes generate a low-$\delta^{13}C$ carbonate reservoir within the subducted slab.

Our model is also compatible with all other observations of melting of carbonated subducted crust and the mineralogy and compositions of inclusions in superdeep diamonds, including the scarcity of carbide and metal (Bulanova et al. 2010, Thomson et al. 2014). Moreover, a study of the coupled behaviour of C and N isotopes in Juina diamonds similarly found evidence for a mixing relationship between crustal and mantle components (Palot et al., 2012). Alternate explanations for the isotopic co-variation we observe are unsatisfactory. The distribution of the data, with a large range in $\delta^{13}C$ while $\delta^{18}O$ remains elevated, demonstrates that O mixes less efficiently than C; in our model this is because the "effective

reaction mixture" that makes up the mantle component is dominated by metal or carbide. Mixing C whilst preserving the crustal $\delta^{18}O$ could be achieved by ingress of a mantle-derived H_2O- and CO_2/carbonate-free fluid into the slab: these chemical constraints rule out all C-bearing fluids except CH_4. Although methane-rich fluids have been associated with diamond formation (Thomassot et al., 2007), they seem improbable for our suite of samples because of the existence of carbonate inclusions (Bulanova et al., 2010; Thomson et al., 2014) that would not be stable with the significantly more reducing conditions required for methane to predominate in the fluid.

Superdeep diamonds from Jagersfontein (South Africa) that host majorite inclusions show a more limited range of $\delta^{13}C$ and $\delta^{18}O$ (Ickert et al., 2015), but nonetheless show a weak negative correlation between the two isotopic systems (Fig. 1). The Ickert et al. (2015) data have slightly lower $\delta^{18}O$ but would otherwise be consistent with similar model parameters to the present study. It has been proposed that the Jagersfontein and Juina-region diamonds relate to Mesozoic subduction off the Gondwanan margin (Harte and Richardson, 2012), and although local variations in the subducted lithology will have been present, the mechanism of diamond formation is expected to be the same. The slope of the correlation is similar to that in the present study, but is offset, suggesting a crustal endmember with lower $\delta^{18}O$ but an otherwise similar mixing relationship occurred in the source region of those samples. The contrast between the smaller range of C and O isotopic compositions in the Jagersfontein samples and the large range in the present study could be due to textural differences in the source region. Conceptually it seems likely that large variations in the ratio of slab to mantle components (and consequently $\delta^{13}C$ and $\delta^{18}O$) could be achieved more readily by mass transport of the slab-derived melt in veins, whereas diffuse, grain-boundary percolation of this melt would result in a more uniform mixing ratio.

The reaction of the carbonate melt with Fe metal or carbide is likely to generate local enrichments in Fe oxide and silicate minerals. Inclusions with high Fe contents are observed in many diamonds from the Juina region, including magnesiowüstite (Fe,Mg)O with Mg# (=Mg/(Fe+Mg)) as low as 0.36 (Kaminsky, 2012) and jeffbenite (formerly called TAPP, tetragonal almandine-pyrope phase) with Mg#

as low as 0.555 (Bulanova et al., 2010); indeed diamond RC2-7 contained an inclusion of the latter with Mg# = 0.61 and a small (10 x 5 μm) touching grain of (Mg, Fe)CO_3, which is consistent with the model advanced above.

In conclusion, the observed oxygen isotopic data for inclusions in superdeep diamonds unambiguously demonstrate that altered oceanic basalts and/or clastic sediments can be retained as an integral part of the slab and descend to the deep upper mantle without being extracted by melting or abrasion by high shear forces at the slab/mantle interface. Interaction of seawater with MORB imparts additional chemical and isotopic signatures. Pb isotopic ratios, δ^7Li and ^{87}Sr/^{86}Sr have all been demonstrated to correlate with δ^{18}O in altered sea floor basalts (Hart et al., 1999; Gao et al., 2012). Given the evidence in this study for an ^{18}O-enriched silicate reservoir in the transition zone, it seems highly likely that the source region for these superdeep diamonds differs from normal mantle with respect to the isotopic ratios of fluid-mobile elements such as Pb, Sr and Li; the high concentrations of incompatible elements in low-degree slab melts (Walter et al., 2008) would efficiently transfer these anomalous isotopic signatures to the surrounding mantle.

Acknowledgements

This work was supported by NERC grant NE/J008583/1 and EIMF award IMF512/2013. Early work by Debora Araujo and Ben Russell identified several of the samples analysed. Analytical support from Stuart Kearns (University of Bristol), John Craven (EIMF) and Adrian Boyce (Scottish Universities Environmental Research Centre) was indispensable. We thank Dan Frost and an anonymous reviewer for helpful comments.

Figure Captions

Fig. 1 Previously reported co-variation of δ^{13}C and δ^{18}O for diamonds and their inclusions worldwide: majoritic (superdeep) garnets from Jagersfontein, South Africa (Ickert et al., 2015), and lithospheric minerals (coesite and garnet) from Argyle, Australia (Schulze et al., 2013), Damtshaa, Botswana (Ickert et al., 2013), Finsch, South Africa (Lowry et al., 1999) and Guaniamo, Venezuela (Schulze et al., 2013).

Fig. 2 Backscattered electron images of a) coesite with exsolved kyanite (Ju5-61), b) garnet of eclogitic affinity with exsolved omphacitic clinopyroxene (Ju5-32) and c) $CaSiO_3$-walstromite with exsolved perovskite (RC2-7).

Fig. 3 Cathodoluminescence image of diamonds a) Ju5-61 and b) Ju5-119 showing complex internal growth structures typical of superdeep diamonds.

Fig. 4 Co-variation of $\delta^{13}C$ and $\delta^{18}O$ for the diamonds and inclusions analysed in the present study and possible fits to the data, indicating the magnitude of the variability of the mixing process: a – $\delta^{18}O^{melt}$ = 11 ‰ and Fe_3C/Mg_2SiO_4 = 2; b – $\delta^{18}O^{melt}$ = 12 ‰ and Fe_3C/Mg_2SiO_4 = 1.5; c – $\delta^{18}O^{melt}$ = 11.5 ‰ and Fe_3C/Mg_2SiO_4 = 2.5; d – $\delta^{18}O^{melt}$ = 11.5 ‰ and Fe_3C/Mg_2SiO_4 = 4. Collectively the possible mixing lines define a “mixing field”. Error bars are 1σ of replicate measurements, where obtained (some are smaller than the data points and are not plotted).

Figure 1

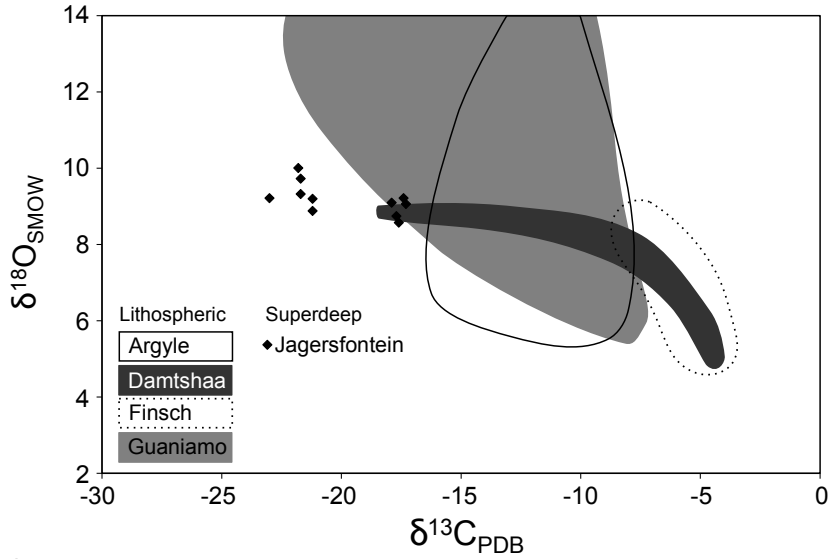

Figure 2

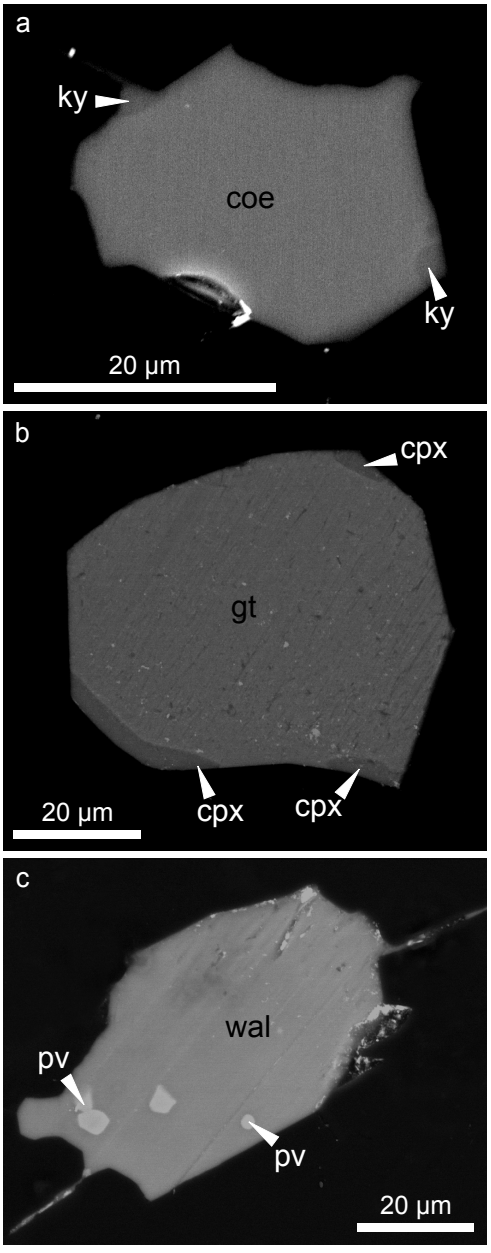

Figure 3

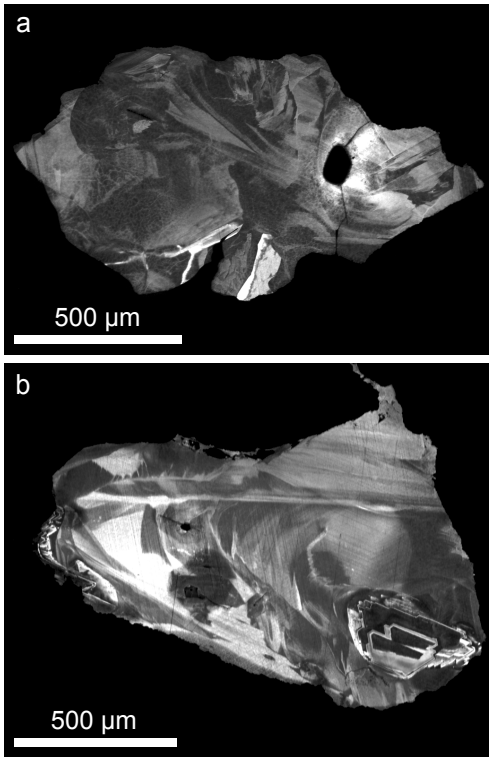

Figure 4 - revised

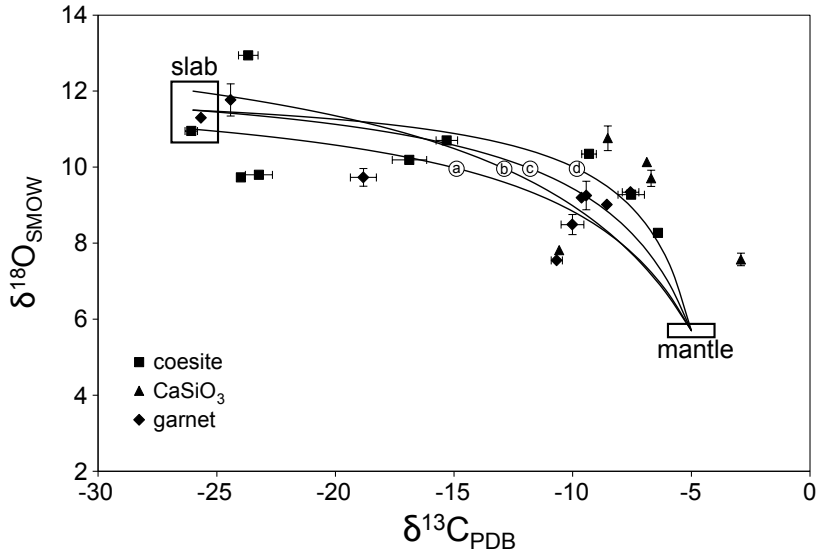

Table 1. A summary of the diamonds and inclusions studied. Carbon isotopic compositions were measured adjacent to the inclusion. Values in parentheses indicate 1σ of replicate analyses (where performed; '0' denotes a value < 0.1 ‰).

Sample name	$\delta^{13}C_{diamond}$	Mineral	$\delta^{18}O_{mineral}$
		Collier-4	
ColN-4	-7.5(6)	coesite[1]	9.3
ColN-7	-6.9(0)	Ca-walstromite[2]	10.1
ColN-10	-10.7(2)	garnet[3]	7.5
ColN-15	-10.6(1)	Ca-walstromite	7.8
ColN-17	-16.9(7)	coesite	10.2
ColN-18-1[4]	-10.0(5)	garnet[3]	8.5(3)
ColN-18-2[4]	-9.6(1)	garnet[3]	9.2
ColN-23	-8.6(1)	garnet	9.0(1)
J14	-6.7(2)	Ca-walstromite[5]	9.7(2)
J17	-9.3(3)	coesite[5]	10.3
J19	-23.7(4)	coesite[1,5]	12.9
RC1-2	-7.6(3)	garnet	9.3(1)
RC2-7	-8.5(1)	Ca-walstromite[2]	10.8(3)
TR1-18A	-6.4(2)	coesite[1]	8.3
		Juina-5	
Ju5-32	-18.8(6)	garnet[3,5]	9.7(2)
Ju5-61	-24.0(1)	coesite[1]	9.7
Ju5-63	-26.1(3)	coesite[1]	10.9
Ju5-82	-24.4(2)	garnet[3]	11.8(4)
Ju5-83	-25.7(1)	garnet[3,5]	11.3
Ju5-89	-23.2(6)	coesite	9.8
Ju5-90	-15.3(5)	coesite[1,5]	10.7
Ju5-119	-9.4(0)	garnet[5]	9.3(4)
		Machado River	
P28	-2.9(1)	Ca-walstromite	7.6(2)

1 – indicates coesite with visible exsolved kyanite

2 – indicates Ca-walstromite with visible exsolved $CaTiO_3$ (perovskite *sensu stricto*)

3 – indicates garnet with exsolved clinopyroxene

4 – two separate (non-touching) inclusions occurring within one diamond; an inclusion of Ca-walstromite was observed by Raman spectroscopy but not exposed or analysed

5 – inclusion previously reported (Bulanova et al., 2010 and Thomson et al., 2014 for Collier-4 and Juina-5 respectively)

Table 2. Compositions of the garnets studied, as determined by EPMA (all Fe as FeO). '0' denotes the element was below the limits of detection (0.01 – 0.02 %); n.a. – not analysed. Asterisks indicate the estimated bulk composition of the garnet prior to exsolution of clinopyroxene.

Sample	SiO_2	TiO_2	Al_2O_3	Cr_2O_3	FeO	MnO	MgO	CaO	Na_2O	K_2O	P_2O_5	Total
ColN-10	40.26	1.58	19.96	0.03	17.44	0.38	7.88	10.71	1.01	0	0.03	99.27
ColN-18-1	40.91	1.40	21.02	0.04	17.41	0.42	8.61	10.69	0.74	0.02	0.01	101.26
ColN-18-2	40.65	1.49	20.89	0.04	17.25	0.40	8.71	10.00	0.88	0.01	0	100.33
ColN-23	38.73	0.78	21.19	0.14	18.68	0.45	9.07	9.24	0.13	0	0.02	98.44
Ju5-32	44.31	0.66	19.17	0.16	12.09	0.28	15.45	7.30	1.34	0	0.06	100.82
Ju5-32*	46.42	0.64	18.55	0.15	11.14	0.26	14.75	6.65	1.43	0.01	n.a.	100
Ju5-82	40.12	0.94	20.16	0.02	15.23	0.56	11.86	6.43	1.03	0.02	0.02	96.39
Ju5-83	40.92	0.65	20.60	0.03	16.56	0.60	11.63	6.75	0.83	0	0.09	98.66
Ju5-83*	44.05	0.71	20.07	0.05	16.20	0.54	11.31	5.91	1.14	0.02	n.a.	100
Ju5-119	38.71	1.29	20.80	0.03	18.32	0.43	7.38	12.46	0.26	0	0.02	99.71
RC1-2	38.79	1.53	20.56	0.06	16.08	0.36	6.91	14.60	0.27	0.02	0.01	99.20

Table 3. Compositions of the Ca-walstromites studied, as determined by EPMA (all Fe as FeO). '0' denotes the element was below the limits of detection (0.01 – 0.02 %).

Sample	SiO_2	TiO_2	Al_2O_3	Cr_2O_3	FeO	MnO	MgO	CaO	Na_2O	K_2O	P_2O_5	Total
ColN-7	50.52	0.03	0.10	0.00	0.21	0.07	0.06	49.05	0.06	0.02	0.03	100.14
ColN-15	51.01	0.03	0.09	0	0.06	0.03	0.04	49.14	0.03	0.03	0.04	100.51
RC2-7	50.67	0.04	0.03	0.02	0.05	0.03	0.00	48.65	0.05	0.03	0.04	99.61
J14	50.38	0.02	0	0	0.20	0.05	0	49.11	0	0	0.02	99.79
P28	51.01	0.01	0.04	0.02	0.15	0.02	0.44	48.56	0.01	0.08	0.04	100.37

References

Alt, J.C. and Teagle, D.A.H. (2003). Hydrothermal alteration of upper oceanic crust formed at a fast-spreading ridge: mineral, chemical, and isotopic evidence from ODP Site 801. *Chemical Geology* **201**, 191-211.

Bindeman, I. (2008). *Oxygen Isotopes in Mantle and Crustal Magmas as Revealed by Single Crystal Analysis*. In K.D. Putirka and F.J. Tepley III (Eds.): Reviews in Mineralogy and Geochemistry 69 – Minerals, inclusions and volcanic processes.

Bulanova, G.P., Smith, C.B., Kohn, S.C., Walter, M.J., Gobbo, L. and Kearns, S. (2008). Machado River, Brazil – a newly recognised ultradeep diamond occurrence. 9th International Kimberlite Conference Extended Abstract No. 9IKC-A-00233.

Bulanova, G.P., Walter, M.J., Smith, C.B., Kohn, S.C., Armstrong, L.S., Blundy, J. and Gobbo, L. (2010). Mineral inclusions in sublithospheric diamonds from Collier 4 kimberlite pipe, Juina, Brazil: subducted protoliths, carbonated melts and primary kimberlite magmatism. *Contributions to Mineralogy and Petrology* **160**, 489-510.

Debret, B., Bolfan-Casanova, N., Padrón-Navarta, J.A., Martin-Hernandez, F., Andreani, M., Garrido, C.J., Sánchez-Vizcaíno, V.L., Gómez-Pugnaire, M.T., Muñoz, M. and Trcera, N. (2015). Redox state of iron during high‐pressure serpentinite dehydration. *Contributions to Mineralogy and Petrology* **169**, 36.

Farquhar, J., Wing, B.A., McKeegan, K.D., Harris, J.W., Cartigny, P. and Thiemens, M.H. (2002). Mass-independent sulfur of inclusions in diamond and sulfur recycling on early Earth. *Science* **298**, 2369-2372.

Fyfe, W.S. (1992). Magma underplating of continental crust. *Journal of Volcanology and Geothermal Research* **50**, 33-40.

Gao, Y., Vils, F., Cooper, K.M., Banerjee, N.., Harris, M., Hoefs, J., Teagle, D.A.H., Casey, J.F., Elliott, T., Laverne, C., Alt, J.C. and Muehlenbacks, K. (2012). Downhole variation of lithium and oxygen isotopic compositions of oceanic crust at East Pacific Rise, ODP Site 1256. *Geochemistry, Geophysics, Geosystems* **13**, 10.

Gregory, R.T. and Taylor, H.P. (1981). An oxygen isotope profile in a section of Cretaceous oceanic crust, Samail Ophiolite, Oman: evidence for $\delta^{18}O$ buffering of the oceans by deep (>5 km) seawater-hydrothermal circulation at mid-ocean ridges. *Journal of Geophysical Research* **86**, 2737-2755.

Hart, S.R., Bluzstan, J., Dick, H.J.B., Meyer, P.S. and Muehlenbachs, K. (1999). The fingerprint of seawater circulation in a 500-meter section of ocean crust gabbros. *Geochimica et Cosmochimica Acta* **63**, 4059-4080.

Harte, B. and Richardson, S. (2012). Mineral inclusions in diamonds track the evolution of a Mesozoic subducted slab beneath West Gondwanaland. *Gondwana Research* **21**, 236-245.

Hudson, J.D. (1977). Stable isotopes and limestone lithification. *Journal of the Geological Society* **133**, 637-660.

Ickert, R.B., Stachel, T., Stern, R.A. and Harris, J.W. (2013). Diamond from recycled crustal carbon documented by coupled $\delta^{18}O$– $\delta^{13}C$ measurements of diamonds and their inclusions. *Earth and Planetary Science Letters* **364**, 85-97.

Ickert, R.B., Stachel, T., Stern, R.A. and Harris, J.W. (2015). Extreme ^{18}O-enrichment in majorite constrains a crustal origin of transition zone diamonds. Geochemical Perspectives Letters **1**, 65-74.

Jacob, D.E. (2004). Nature and origin of eclogite xenoliths from kimberlites. *Lithos* **77**, 295-316.

Kaminsky, F. (2012). Mineralogy of the lower mantle: A review of 'super-deep' mineral inclusions in diamond. *Earth Science Reviews* **110**, 127-147.

Kaminsky, F.V., Sablukov, S.M., Belousova, E.A., Andreazza, P., Tremblay, M. and Griffin, W.L. (2010). Kimberlitic source of super-deep diamonds in the Juina area, Mato Grosso State, Brazil. *Lithos* **114**, 16-29.

Kiseeva, E.S., Litasov, K.D., Yaxley, G.M., Ohtani, E. and Kamenetsky, V.S. (2013). Melting and phase relations of carbonated eclogite at 9–21 GPa and the petrogenesis of alkali-rich melts in the deep mantle. *Journal of Petrology* **54**, 1555-1583.

Kubo, A., Suzuki, T. and Akaogi, M. (1997). High pressure phase equilibria in the system $CaTiO_3$-$CaSiO_3$: stability of perovskite solid solutions. *Physics and Chemistry of Minerals* **24**, 488-494.

Land, L.S. and Lynch, F.L. (1996). $\delta^{18}O$ values of mudrocks: more evidence for an ^{18}O-buffered ocean. *Geochimica et Cosmochimica Acta* **60**, 3347-3352.

Liu, L., Zhang, J., Green, H.W., Jin, Z. and Bozhilov, K.N. (2007). Evidence of former stishovite in metamorphosed sediments, implying subduction to >350 km. *Earth and Planetary Science Letters* **263**, 180-191.

Lowry, D., Mattey, D.P. and Harris, J.W. (1999). Oxygen isotope composition of syngenetic inclusions in diamond from the Finsch Mine, RSA. *Geochimica et Cosmochimica Acta* **63**, 1825-1836.

Luth, R.W. and Stachel, T. (2014). The buffering capacity of lithospheric mantle: implications for diamond formation. *Contributions to Mineralogy and Petrology* **168**, 1083.

Nadeau, S., Phillipot, P. and Pineau, F. (1993). Fluid inclusion and mineral isotopic compositions (H-C-O) in eclogitic rocks as tracers of local fluid migration during high-pressure metamorphism. *Earth and Planetary Science Letters* **114**, 431-448.

Page, F.Z., Kita, N.T. and Valley, J.W. (2010). Ion microprobe analysis of oxygen isotopes in garnets of complex chemistry. *Chemical Geology* **270**, 9-19.

Palot, M., Cartigny, P., Harris, J.W., Kaminsky, F.V. and Stachel, T. (2012). Evidence for deep mantle convection and primordial heterogeneity from nitrogen and carbon stable isotopes in diamond. *Earth and Planetary Science Letters* **357-358**,179-193.

Rohrbach, A. and Schmidt, M.W. (2011). Redox freezing and melting in the Earth's deep mantle resulting from carbon–iron redox coupling. *Nature* **472**, 209-212.

Rohrbach, A., Ghosh, S., Schmidt, M.W., Wijbrans, C.H. and Klemme, S. (2014). The stability of Fe–Ni carbides in the Earth's mantle: Evidence for a low Fe–Ni–C melt fraction in the deep mantle. *Earth and Planetary Science Letters* **388**, 211-221.

Schulze, D.J., Harte, B., Valley, J.W., Brenan, J.M. and Channer, D. M. de R. (2003). Extreme crustal oxygen isotope signatures preserved in coesite in diamond. *Nature* **423**, 68-70.

Schulze D.J., Harte, B., Valley, J.W. and Channer, D.M.DeR. (2004). Evidence of subduction and crust–mantle mixing from a single diamond. *Lithos* **77**, 349-358.

Schulze, D.J., Harte, B., EIMF, Page, F.Z., Valley, J.W., Channer, D.M.DeR. and Jaques, A.L. (2013). Anticorrelation between low $\delta^{13}C$ of eclogitic diamonds and high $\delta^{18}O$ of their coesite and garnet inclusions requires a subduction origin. *Geology* **41**, 455-458.

Sharp, Z.D., Essene, E.J. and Smyth, J.R. (1992). Ultra-high temperatures from oxygen isotope thermometry of a coesite-sanidine grospydite. *Contributions to Mineralogy and Petrology* **112**, 358-370.

Shilobreeva, S., Martinez, I., Busigny, V., Agrinier, P. and Lavergne, C. (2011). Insights into C and H storage in the altered oceanic crust: Results from ODP/IODP Hole 1256D. *Geochimica et Cosmochimica Acta* **75**, 2237-2255.

Smart, K.A., Chacko, T., Stachel, T., Tappe, S., Stern, R.A., Ickert, R.B. and EIMF (2012). Eclogite formation beneath the northern Slave craton constrained by diamond inclusions: Oceanic lithosphere origin without a crustal signature. *Earth and Planetary Science Letters* **319**-**320**, 165-177.

Stachel, T., Brey, G.P. and Harris, J.W. (2005). Inclusions in sublithospheric diamonds: glimpses of deep Earth. *Elements* **1**, 73-78.

Stakes, D.S. and O'Neil, J.R. (1982). Mineralogy and stable isotope geochemistry of hydrothermally altered oceanic rocks. *Earth and Planetary Science Letters* **57**, 285-304.

Thomassot, E., Cartigny, P., Harris, J.W. and Viljoen, K.S. (2007). Methane-related diamond crystallization in the Earth's mantle: stable isotope evidences from a single diamond-bearing xenolith. *Earth and Planetary Science Letters* **257**, 362-371.

Thomson, A.R., Kohn, S.C., Bulanova, G.P., Smith, C.B., Araujo, D., EIMF and Walter, M.J. (2014). Origin of sub‐lithospheric diamonds from the Juina-5 kimberlite (Brazil): constraints from carbon isotopes and inclusion compositions. *Contributions to Mineralogy and Petrology* **168**, 1081.

Walter, M.J., Bulanova, G.P., Armstrong, L.A., Keshav, S., Blundy, J.D., Gudfinnsson, G., Lord, O.T., Lennie, A.R., Clark, S.M., Smith, C.B. and Gobbo, L. (2008). Primary carbonatite melt from deeply subducted oceanic crust. *Science* **454**, 622-625.

Walter, M.J., Kohn, S.C., Araujo, D., Bulanova, G.P., Smith, C.B., Gaillou, E., Wang, J., Steele, A. and Shirey, S.B. (2011). Deep mantle cycling of oceanic crust: evidence from diamonds and their mineral inclusions. *Science* **334**, 54-57.

Widiyantoro, S., Kennett, B.L.N. and van der Hilst, R.D. (1999). Seismic tomography with P and S data reveals lateral variations in the rigidity of deep slabs. *Earth and Planetary Science Letters* **173**, 91-100.

Yang, X.-Y., Zheng, Y.-F., Liu, D. and Dai, J. (2001). Chemical and carbon isotope compositions of fluid inclusions in peridotite xenoliths and eclogites from eastern China: geodynamical implications. *Physics and Chemistry of the Earth (A)* **26**, 705-718.

Zhang, J., Liebermann, R.C., Gasparik, T. and Herzberg, C.T. (1993). Melting and subsolidus relations of SiO_2 at 9-14 GPa. *Journal of Geophysical Research* **98**, 19785-19793.